Available online at www.sciencedirect.com
SCIENCE DIRECT®
Journal of Computational Physics 193 (2003) 180–197
JOURNAL OF COMPUTATIONAL PHYSICS
www.elsevier.com/locate/jcp

Further study on the high-order double-Fourier-series spectral filtering on a sphere

Hyeong-Bin Cheong *, In-Hyuk Kwon, Tae-Young Goo

Department of Environmental Atmospheric Sciences, Pukyong National University, 599-1 Daeyeon 3-dong, Nam-gu, Busan 608-737, Republic of Korea

Received 13 January 2003; received in revised form 3 June 2003; accepted 31 July 2003

Abstract

A high-order harmonic spectral filter (HSF) is further studied using double Fourier series (DFS), which performs filtering in terms of successive inversion of tridiagonal matrices with complex-valued elements. The high-order harmonics filter equation is split into multiple Helmholtz equations. It is found that the filter provides the same order of accuracy as the spectral filter in [J. Comput. Phys. 177 (2002) 313] that consists of the pentadiagonal matrices with real-valued elements. The advantage of the filter over the previous one lies on the simplicity and easiness of numerical implementation or computer coding, just requiring the same complexity as Poisson's equation solver. However, the operation count associated with the filter increases by a factor of about 2. To circumvent the inefficiency while preserving the simplicity, an easy way to construct pentadiagonal matrices associated with the biharmonic equation is presented in which the tridiagonal matrices related with Poisson's equation are manipulated. Computational efficiency of the spectral filter is discussed in terms of the relative computing time to the spectral transform. It is revealed that the computing cost (requiring $O(N^2)$ operations with N being the truncation) for the spectral filtering, even with the complex-valued matrices, is not significant in the DFS spectral model that is characterized by $O(N^2 \log_2 N)$ operations. Filtering with different DFS expansions is discussed with a focus on the accuracy and pole condition. It is shown that the DFS violating the pole conditions produces a discontinuity at poles in case of wave truncation, and its influence spreads over the globe. The spectral filter is applied to two kinds of uniform-grid data, the regular and the shifted grids, and the results are compared with each other. The operator splitting (or spherical harmonics factorization) makes it feasible to apply the finite difference method to the high-order harmonics filter with ease because only the five-point stencil computations are required. The application could also be extended to other numerical methods only if the Helmholtz equation solver is available.

AMS: 65Fxx; 65Txx; 76Mxx

Keywords: High-order harmonic spectral filter; Double Fourier series; Smoothing; Tridiagonal matrix; Pentadiagonal matrix; Operator spiltting; Spherical surface

* Corresponding author. Tel./fax: +82-51-620-6286.
E-mail address: hbcheong@pknu.ac.kr (H.-B. Cheong).

0021-9991/$ - see front matter
doi:10.1016/j.jcp.2003.07.029

1. Introduction

High-order harmonic spectral filter with DFS was presented (hereafter referred to as HSF-DFS) for a smoothing (*or* filtering) of spherical surface data [8]. HSF-DFS performs filtering in terms of inversion of pentadiagonal matrices whose elements are real-valued DFS spectral coefficients associated with the high-order implicit diffusion equation. The harmonic spectral filter with DFS, i.e., the Helmholtz equation solver, can be found in [7]. DFS (high-order) harmonic spectral filter provides an isotropic filtering on the sphere as the spherical harmonics filter [2,6,8,19,21] does. It requires only $O(N^2)$ operations in spectral space in contrast to $O(N^3)$ operations needed for the spherical harmonics filter, where N is the truncation. As the order of the filter (i.e., the order of the Laplacian operator) increases, a sharper cutoff of the high-wavenumber spherical-harmonics component is achieved but the operation count increases almost linearly with the order. Unlike the projection operators as in [6,23], the diffusive-type spectral filter such as HSF-DFS cannot completely eliminate high-wavenumber spherical-harmonics components from the grid- or wave-data. Applications to time-dependent nonlinear problems have shown that HSF-DFS is useful as a numerical stabilizer for the DFS spectral model that is characterized by $O(N^2 \log_2 N)$ operations, because it can control the noises with computational efficiency without affecting the physics of the problem. It is particularly useful, as discussed in [8], when an explicit incorporation of the scale-selective viscosity is not feasible due to either a difficulty in numerical implementation or a restriction to the viscosity coefficient.

Though not shown, the spectral filter with pentadiagonal matrices may be extended to the mixed order filter, i.e., the filter equation having multiple Laplacian operators with different order, only if the requirement for the filter coefficients is satisfied [8]. The mixed order filter provides a more flexible, wavenumber-dependent smoothing effect that is not available for the usual single-harmonic-operator filter. An arbitrary scale-selectivity can be accomplished only for the spherical harmonics filter [2,10,21]: Once the spectral component is calculated, a filter of arbitrary functional form of the total wavenumber may be implemented although the biharmonic diffusion (or viscosity) is most commonly used in the time-dependent model [14,20,22].

The pentadiagonal matrices are the most important factors for the efficient high-order harmonic filter in [8]. The matrices are, however, constructed via rather a complicated procedure and their elements include many terms of fourth-order polynomials of the meridional wavenumber. As a result, though not serious, a relatively long computer code is necessary for the filter. To keep the simplicity of the DFS model and at the same time to provide an easy numerical implementation for practical use, it would be desirable to introduce matrices associated with the filter as simple as possible unless the computational efficiency and accuracy are lost. To meet this necessity, in this study a new HSF-DFS is proposed that performs in terms of successive inversion of the Helmholtz equations with the complex-valued coefficients. The filter equation with a high-order Laplacian-operator type is split into multiple Helmholtz equations. The matrices that should be prepared for this filter are all tridiagonal ones associated with the Laplacian operator instead of the pentadiagonal matrices. Therefore, the new filter can be implemented with much more ease than the filter in [8]. However, the computing time is nearly doubled because the matrix elements are complex valued. To circumvent this inefficiency while preserving the simplicity, another high-order filter is designed which inverts pentadiagonal matrices. The pentadiagonal matrices in the filter are the same as those in [8]. The new aspect associated with the filter is the simplicity and easiness to construct the matrices. The idea of splitting of high-order harmonic operator into simple Helmholtz equations may be extended to other numerical methods, e.g., finite difference method and finite element method, because only the second order differential equations (Helmholtz equations) are solved.

In pursuit of an efficiency and accuracy, the double Fourier series has been applied to various problems (e.g. [9,16]). This reflects a high potential of the DFS spectral method as a promising alternative to the spherical-harmonics approach in various fields. When selecting the basis functions for the DFS spectral method, the pole conditions are of primary importance. In the case of basis functions violating the pole

conditions [1,3,17,25], a discontinuity of the data field may occur at poles. Since the basis function is of global-defined, the influence due to discontinuity may spread over the sphere. In spite of the importance, such an issue has not been reported in detail.

The paper is organized as following. In the next section, a new high-order HSF-DFS is presented for the uniform spherical grid systems, the regular and shifted grids. The issue of completeness for the DFS expansion is discussed along with an effective way for the spectral transform in the case where the polar singularity exists. In Section 3 tests with the spherical harmonics are given. Two DFS methods are compared in some detail with a focus on the influence of the truncation. Section 4 is devoted to the derivation of a simple way to construct the pentadiagonal matrices for the efficient HSF-DFS used in [8]. Summary and conclusions are presented in the final section.

2. High-order harmonic spectral filter with tridiagonal matrices

2.1. High-order harmonic filter equation and the uniform-grid system

The harmonic filter equation of order q (being a positive integer) over a unit sphere is written as

$$[1 + v(-1)^q \nabla^{2q}]w = g, \tag{2.1}$$

where

$$\nabla^2 \equiv \frac{1}{\sin\phi}\frac{\partial}{\partial\phi}\sin\phi\frac{\partial}{\partial\phi} + \frac{1}{\sin^2\phi}\frac{\partial^2}{\partial\lambda^2}$$

with λ being longitude and $\phi = \pi/2 +$ latitude, respectively, and v is a positive-valued filter coefficient. The variable $g(\lambda,\phi)$ is a given forcing function and $w(\lambda,\phi)$ is the filtered function. If the forcing function $g(\lambda,\phi)$ is real (complex), $w(\lambda,\phi)$ must be real-valued (complex-valued) in the filter equation. With the sign of v given negative (2.1) becomes a reverse diffusion equation, which is used in various problems, e.g., the chemical reactions including the upgradient diffusion [12] or the image processing [4].

It is assumed that $g(\lambda,\phi)$ and $w(\lambda,\phi)$ are defined at grid points with a uniform longitude–latitude spacing. Fig. 1 illustrates two kinds of uniform latitude–longitude grid on a spherical surface, which are different from each other in the meridional location of grid points. One is the regular grid system including the poles and the Equator while the other is the shifted grid system where the poles and the Equator are not the data point. For convenience, we refer to the former as R-grid and the latter S-grid, respectively. R-grid

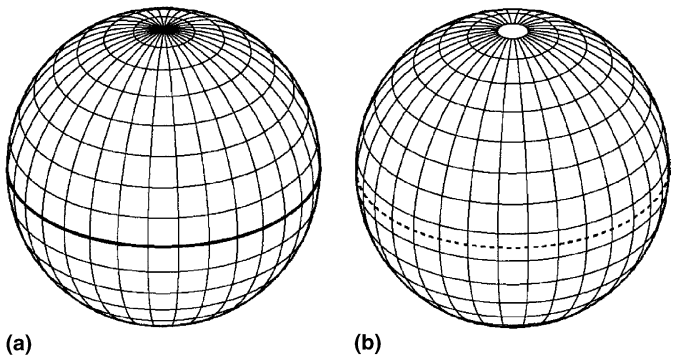

Fig. 1. Spherical grid system with uniform angular spacing. The data points include the equator and poles for (a), but not for (b).

is of a very familiar structure because most of the global dataset used for the weather and climate analysis are arranged in this form [11], while S-grid is mainly used in numerical models [1,6–9,17,23]. The filter operator in (2.1) can be split into multiple Helmholtz equations with complex coefficient, i.e.,

$$[1-\gamma_1\nabla^2][1-\gamma_2\nabla^2]\cdots[1-\gamma_q\nabla^2]w = g, \tag{2.2}$$

where

$$\gamma_p = \nu^{1/q}\exp\left[\frac{s\pi\mathrm{i}+2\pi(p-1)\mathrm{i}}{q}\right] \quad (\mathrm{i}=\sqrt{-1},\ p=1,2,\ldots,q), \tag{2.3}$$

with $s=0$ ($s=1$) for $q=$ odd (even), respectively. Complex constants γ_p are obtained as the solution of $\gamma^q+\nu(-1)^q=0$, where the subscript p denotes the pth solution.

Filtering of $g(\lambda,\phi)$ is accomplished by successive q-times inversions of the Helmholtz equations with complex coefficient, starting from

$$[1-\gamma_1\nabla^2]w_1 = g, \tag{2.4}$$

where

$$w_1 = [1-\gamma_2\nabla^2]\cdots[1-\gamma_q\nabla^2]w. \tag{2.5}$$

2.2. Double-Fourier-series expansion and completeness

In this study, any scalar function, e.g., $g(\lambda,\phi)$ is defined at the sampling points (λ_k,ϕ_j) with uniform longitude–latitude spacing ($K=2N,\ N=$ even)

$$\begin{aligned}
&\lambda_k = 2\pi k/K, \quad k=0,1,\ldots,K-1,\\
&\phi_j = \pi j/N, \quad j=0,1,\ldots,N \text{ for R-grid},\\
&\phi_j = \pi(j+0.5)/N, \quad j=0,1,\ldots,N-1 \text{ for S-grid}.
\end{aligned} \tag{2.6}$$

It is obvious that $g(\lambda_k,\phi_0)$ and $g(\lambda_k,\phi_N)$ are independent of k for the R-grid, because they represent the same data point. Note that *the actual number of data points* is $K(N-1)+2$ and KN for the R-grid and S-grid, respectively.

Let $\{g_m^{\mathrm{c}}(\phi), g_m^{\mathrm{s}}(\phi)\}$ be the zonal cosine and sine transform of $g(\lambda,\phi)$:

$$g(\lambda,\phi) = \sum_{m=0}^{K/2} g_m^{\mathrm{c}}(\phi)\cos m\lambda + \sum_{m=0}^{K/2-1} g_m^{\mathrm{s}}(\phi)\sin m\lambda, \tag{2.7}$$

where m is the zonal wavenumber. Hereafter, the superscripts 'c' and 's' are dropped for convenience. The boundary condition at poles for $g_m(\phi)$ in [6] is schematically illustrated in Fig. 2. The simplest meridional expansion functions appropriate for the pole conditions are as follows [6–8]:

$$g_m(\phi) = \begin{cases} \sum_{n=0}^{N_{\mathrm{o}}} g_{n,m}\cos n\phi & \text{for } m=0,\\ \sum_{n=1}^{N_{\mathrm{s}}} g_{n,m}\sin n\phi & \text{for odd } m,\\ \sum_{n=1}^{N_{\mathrm{c}}} g_{n,m}\sin\phi\sin n\phi & \text{for even } m(\neq 0). \end{cases} \tag{2.8a, b, c}$$

The number of meridional expansion coefficients must be given as large as can guarantee the completeness of the Fourier expansion (that is, as can reconstruct accurately the given grid-data with the expansion coefficients)

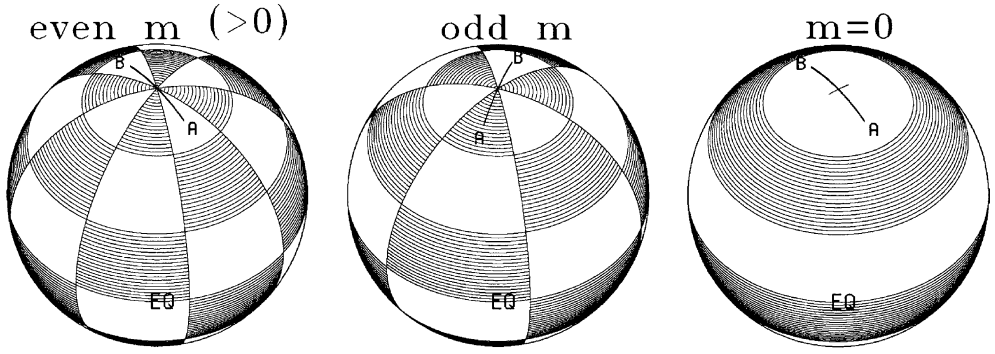

Fig. 2. Schematic illustration of the necessary boundary conditions at poles [6] for the zonal Fourier transform of a scalar variable, $g_m(\phi)$. The dark region indicates the negative value, and the wavy structure in the meridional direction is chosen arbitrarily. Considering a great-circle arc (from A to B) passing over the pole, both g_m and its meridional derivative vanish for even $m(\neq 0)$, while g_m vanishes but the derivative does not for odd m. Pole conditions for $m = 0$ are the reversed sense of the odd-m case.

$$(N_o, N_s, N_c) = \begin{cases} (N, N-1, N-1) & \text{for R-grid,} \\ (N-1, N, N) & \text{for S-grid.} \end{cases} \tag{2.9}$$

The total number of expansion coefficients is

$$N_o + 1 + N_s(K/2 - 1) + N_c K/2, \tag{2.10}$$

which gives $K(N-1)+2$ and KN for the R-grid and S-grid, respectively. It is worthy of noting that the number of expansion coefficients are exactly the same as that of *the physical data points*. This means the appropriateness of the wave truncation or the equivalence of informations available from both data. In other words, the Parseval identity holds for the case of DFS spectral expansion on the sphere, as was illustrated in [6] in the form of global averaging of a quadratic term. As will be stated in appendix, the parity function for even zonal wavenumber does not cause the aliasing.

Another type of double Fourier series, introduced by Orszag [17] and used for Poisson's equation by Yee [25], may be applied to the filter equation, though not satisfying the pole conditions for even $m(\neq 0)$:

$$g_m(\phi) = \begin{cases} \sum_{n=0}^{N_o} g^*_{n,m} \cos n\phi & \text{for even } m, \\ \sum_{n=1}^{N_s} g_{n,m} \sin n\phi & \text{for odd } m, \end{cases} \tag{2.11a, b}$$

where the superscript '*' was used to discern from the spectral coefficients for modified sine series in (2.8c). The truncation limits must be given the same as in the case of (2.8).

Spectral coefficients are obtained by usual half-ranged cosine or sine transform [18]. For the modified sine series (2.8c), a variable transform $g^{(S)}_m(\phi) \equiv g_m(\phi)/\sin\phi$ must be done to facilitate the fast sine transform. However, this cannot be applied to the R-grid because the division by $\sin\phi$ is impossible at poles. This difficulty is overcome by replacing the modified sine series by cosine series, which is presented in Appendix A along with the issue of pole condition for the cosine series.

It is emphasized that for S-grid system, unlike the R-grid system presented in Appendix A, the cosine series is not equivalent to the modified sine series. In case where the modified sine series is replaced by the cosine series with the recursion relations as in (A.2a) and (A.2b), the largest wavenumber $N_o(\equiv N-1)$ of (2.11a) that should be the same as (N_c+1), becomes greater than the grid number N between poles by 2. This gives rise to an aliasing. With only the last wave components dropped, the modified sine series becomes equivalent to the cosine series. This invites a difference in accuracy between the two series:

the modified sine series must be more accurate than the cosine series to the extent that the largest wave components $\sin\phi\sin(N-1)\phi$ and $\sin\phi\sin N\phi$ project on to the data field. Tests on the aliasing will be given in the following section.

2.3. Inversion of Helmholtz equation with a complex coefficient

Solution method of the Helmholtz equation with a complex coefficient is basically the same as that having a real-valued coefficient. One major difference is the computational aspect that more operations and array space are needed in the present case, because the variables must be defined in complex-valued array. During the inversions in (2.2), the solution of a Helmholtz equation is substituted in the next inversion step as a forcing function. While the new forcing function may become complex-valued (i.e., if γ_1 is complex, w_1 in (2.4) is complex even when g is real), the final solution associated with the last inversion step, i.e., the filtered function w must be real valued. Therefore, the filtered function corresponds to the real part of the solution for the last inversion step.

As a strategy to optimize the computations involved in the filter equation (2.2), it would be desirable to filter two variables at the same time. This is done by combining two variables into a complex variable for zonal sine- or cosine-Fourier transforms, separately. More conveniently, the zonal cosine and sine transform of a variable, say $\{g_m^{\mathrm{c}}(\phi), g_m^{\mathrm{s}}(\phi)\}$, may be combined into a complex column vector. By doing so, the operation count for the new method can be suppressed to be about two times of the pentadiagonal-matrix case in [8].

As was shown in [6,7,25], the Helmholtz equation in (2.4) is multiplied by $\sin^2\phi$ and then substituted with the DFS expansion to yield the tridiagonal matrix equations for odd and even n, separately

$$[A-\gamma_1 D]\mathbf{w} = A\mathbf{g}, \tag{2.12}$$

where the matrices A and D are tridiagonal matrices, and $\mathbf{w}$ and $\mathbf{g}$ being the column vectors consisting of the spectral components. The sizes of A and D are given in Table 1, which depend on both the grid system and the expansion functions. The matrix components for A and D are easily calculated with recursion formula of the trigonometric functions. To facilitate an immediate use the matrix components are presented in Fig. 3. With γ_1 being complex valued, the matrix $H(\equiv A-\gamma_1 D)$ becomes also complex.

The global integral of $w_1(\lambda,\phi)$ (and also w) should be the same as that of $g(\lambda,\phi)$. Thus, as was done in [7], after the inversion is finished, the component $(w_1)_{0,0}$ is modified so that the global integral is the same for both variables. Since none of the expansion functions in (2.8a) alone cannot represent the global-mean unlike the spherical harmonics expansion, $(w_1)_{0,0}$ is modified using $(w_1)_{n,0}$ with n being even:

$$[g]-\sum_{n=1}^{N_H}\frac{(w_1)_{2n,0}}{1-(2n)^2}\Rightarrow (w_1)_{0,0}, \tag{2.13}$$

Table 1
Size of matrices A and D of the tridiagonal system for even n with the definition given by $N_2 = N/2$, $N_{2p} = N_2+1$ and $N_{2m} = N_2-1$

m	R-grid		S-grid
	Cheong [Eq. (2.8)]	Yee–Orszag [Eq. (2.11)]	
0	$N_{2p}\times N_{2p}$	$N_{2p}\times N_{2p}$	$N_2\times N_2$
$1,3,\ldots$	$N_{2m}\times N_{2m}$	$N_{2m}\times N_{2m}$	$N_2\times N_2$
$2,4,\ldots$	$N_{2m}\times N_{2m}$	$N_{2p}\times N_{2p}$	$N_2\times N_2$

Matrix size with odd n is $N_2\times N_2$ for all cases.

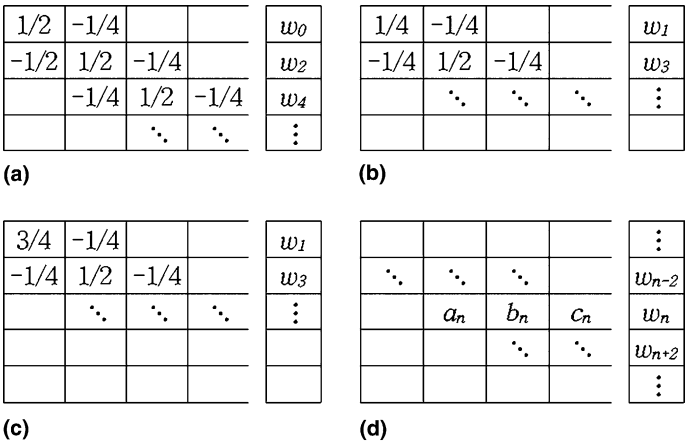

Fig. 3. (a, b) Matrix components of A for cosine series. (c) Matrix components of A for sine and modified sine series. All other elements not shown above are 1/2 and −1/4 for the diagonal and off-diagonal components, respectively. (d) Matrix components of D. For sine and cosine series $a_n = (n-1)(n-2)/4$, $b_n = -n^2/2 - m^2$ and $c_n = (n+1)(n+2)/4$, while for the modified sine series (2.8c) $a_n = n(n-1)/4$, $b_n = -n^2/2 - m^2$ and $c_n = n(n+1)/4$. For more details refer to [6]. The column vector associated with the matrix is shown on the right-hand side of each figure.

$$[g] = \sum_{n=0}^{N_H} \frac{g_{2n,0}}{1-(2n)^2}, \tag{2.14}$$

where $N_H = N_o/2$ and the square bracket denotes the global averaging. This procedure is necessary only at the last Helmholtz-equation solver.

3. Tests results

3.1. Tests with spherical harmonic functions

Accuracy of Poisson's equation solver using DFS was presented by Cheong [6] for (2.8) and by Yee [25] for (2.11). The accuracy of the Helmholtz-equation solver may be basically the same as the Poisson's equation. For the tests on the HSF-DFS, the forcing function for which the solution of (2.1) is known is introduced

$$g = w + vG, \tag{3.1}$$

$$w = \begin{cases} (1+\cos\phi)(\sin\phi)^m \cos m\lambda, & m \neq 0, \\ \cos\phi + \cos 2\phi, & m = 0, \end{cases} \tag{3.2}$$

$$G = \begin{cases} \left(c_m^q + c_{m+1}^q \cos\phi\right)(\sin\phi)^m \cos m\lambda, & m \neq 0, \\ (-2)^q \cos\phi + (-6)^q (1 + 3\cos 2\phi), & m = 0, \end{cases} \tag{3.3}$$

where $c_m = -m(m+1)$. The computations for tests are carried out with double precision. For each zonal wavenumber, the normalized error is evaluated by

$$E = \frac{[|w_c - w|]}{[|w|]}, \tag{3.4}$$

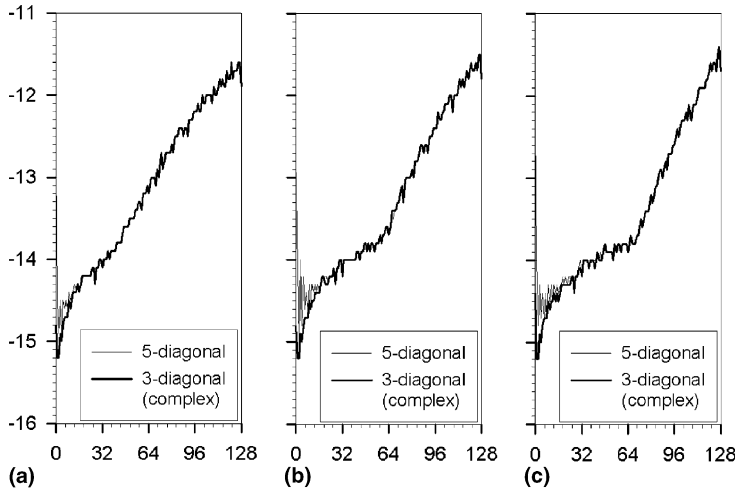

Fig. 4. Comparison of the harmonic spectral filters for $K \times J = 256 \times 128$. The thin (thick) line represents the filter with pentadiagonal (complex tridiagonal) matrix. (a), (b) and (c) correspond to the second, third- and fourth-order filter (i.e., $q = 2$, 3 and 4), respectively. The abscissa denotes the zonal wavenumber and the filter coefficients are given as $100/(128 \times 129)^q$.

where the square bracket implies the global mean and w_c is the inverted value. In Fig. 4, $\log_{10} E$ is plotted for the harmonics order of 2, 3 and 4, where the filter viscosity is given $v = 100/[N(N+1)]^q$ with $N = 128$. Note that the method of [8] and the new method give almost the same results with the accuracy being slightly increased for the new method. For low zonal wavenumbers, the error decreases as the harmonics order increases because of decreasing filter viscosity at high orders. This is consistent with the case of biharmonic equation solver shown in [6] where the error associated with the inversion of Helmholtz–Poisson type becomes large as the relative importance of the biharmonic- to the harmonic term increases.

In Fig. 5, the errors for the two types of DFS are compared for different grid systems, where the inversion is carried out with the new method. The resolution is the same as in Fig. 4 and the fourth-order filter is used. Since for $m =$ odd and $m = 0$ the expansion functions are the same, the errors for DFS used in [6] (denoted as 'Cheong S-grid') are shown only for $m =$ even$(\neq 0)$. The errors exhibit the same order for all cases except for 'Cheong S-grid' case which shows a slightly improved accuracy compared to other cases. (The lines for R-grid are almost overlapped to the thick line.)

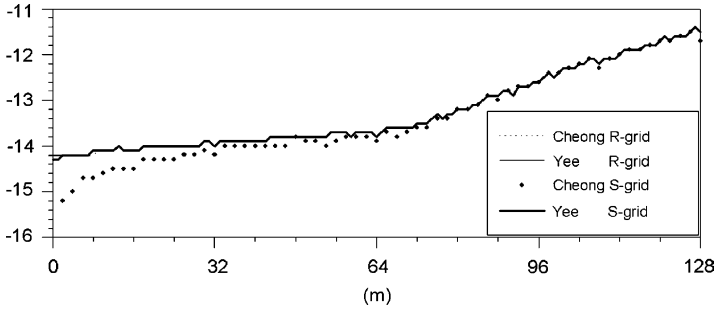

Fig. 5. Comparison of the harmonic spectral filters for different DFS and grid system, where m is the zonal wavenumber. All filters consist of tridiagonal matrix solver and the order of the filter is 4. The resolution and filter coefficient are the same as in Fig. 4.

3.2. Difference between two DFSs in (2.8) and (2.11)

It is not considered that the differences shown in Figs. 4 and 5 are quite significant because the differences are observed where the errors are close to the machine roundoffs. Rather, it would be meaningful to see a difference for a general case, e.g., an arbitrary forcing function. It is of particular interest in this section to see the differences between the expansion functions (2.8) and (2.11) for S-grid. As stated in Section 2, the modified sine series (2.8c) can resolve more wave components for S-grid than the cosine series by two level. To demonstrate this, the Legendre function $P^m_{m+2}(\mu)$ with μ being sine of latitude is adopted as the forcing function. The function becomes an aliased mode because the Gaussian quadrature is exact up to the polynomial degree of $N-1$ when the number of grids between poles is set N. For a clarity, N is given as small as possible, e.g., $N=8$, for which the aliasing occurs with $m>5$. The error measure $\log_{10} E$ is presented in Table 2(a). The difference between two expansions is clear: for $m=6$, the error for (2.8c) is near the machine rounding while the error for (2.11a) is larger than $O(10^{-2})$. As an extension to an arbitrary field for comparison, a forcing function of cosine bell is introduced

$$g(r)=\begin{cases}[1+\cos(\pi r/r_m)]/2, & r\leqslant r_m,\\ 0, & r>r_m,\end{cases} \tag{3.5}$$

where $r_m=\pi/10$ and r is the arclength between the grid point and the center (180E, 10N). The forcing function is filtered with $q=4$, i.e., a fourth-order filter, where the filter coefficient is the same as in Fig. 5. The normalized global average of difference between two filtered fields is shown in Table 2(b). The difference for $N=8$ is as large as $O(10^{-2})$ and it decreases exponentionally as the resolution increases, showing a convergence property typical of the spectral method.

It is often necessary to truncate a part of the wave coefficients when reconstructing the grid point value through spectral transform. The most important example of this may be the 2/3 rule for the evaluation of quadratic terms [5–7,10,14,19,23]. Unlike the spherical-harmonics spectral method the expansion functions in (2.8) and (2.11) are not isotropic although the filtering with them based on the Laplacian operator provides isotropic results on the sphere as shown in [8]. Thus, elimination of the high wavenumber components may result in the anisotropic field. In case of the DFS in (2.11) with the R-grid system the reconstructed grid point data after the truncation becomes multi-valued at poles. However, since the pole is a grid point for R-grid, any function must be single-valued there. Thus, the truncation may produce unphysical grid data unless an appropriate filter, not a diffusive-type but a spherical-harmonics projection operator, is applied to the DFS spectral space before transforming to the grid data. (The unphysical grid data at poles may be used in computation without any problem because the spherical grid data are handled usually as two dimension array.) To use the spherical-harmonics projection, the eigenvectors of the matrix $D^{-1}A$ associated with the R-grid must be calculated and stored as was done in [6]. The projection operator is computationally inefficient, requiring $O(N^3)$ operations. Another approach is attempted by [15] to avoid

Table 2
(a) Logarithmic error ($\log_{10} E$) associated with the fourth-order harmonic filtering (inversion) of the Legendre function $P^m_{m+2}(\mu)$ with μ being sine of latitude. The resolution for the test is set $K=16$. (b) Normalized difference between the filtered fields of cosine bell in (3.5) by the expansions (2.8) and (2.11), respectively

m	Cheong [Eq. (2.8)]	Yee–Orszag [Eq. (2.11)]	m	Normalized difference
(a)			(b)	
0	−15.06	−15.06	8	0.108E − 01
2	−15.13	−15.12	16	0.365E − 03
4	−14.42	−14.37	32	0.119E − 04
6	−13.11	−1.78	64	0.209E − 05
8	−1.47	−1.01	128	0.104E − 06

the discontinuity at poles and anisotropicity caused by the truncation for the R-grid system, where the truncated wave data are transformed in meridian to the grid data and then the projection is carried out.

For the DFS in (2.11), another undesirable problem is expected to be observed near the poles because the remaining components after truncation for even zonal wavenumber other than zero do not satisfy the pole condition in (A.4). In relation with the truncation, it would be of interest to focus on the case where both the truncation and the filtering are done. It is desired that the results are the same regardless of the order as in the spherical-harmonics model.

In Fig. 6, such issues are well illustrated: the field of cosine bell shape (Fig. 6(a)), as defined by (3.5), with the resolution of $N = 32$ ($\equiv 64 \times 32$grids) is transformed to two different wave spaces using (2.8) and (2.11), respectively. Then the amplitude of the wave component is made zero for either $m > N/2$ or $n > N/2$. The grid data transformed from the remaining wave components are presented in panels 6b and 6c. Systematic noise-like patterns of small scale are found in Fig. 6(c) while not in the panel 6b. Panels 6d and 6e compare the results of both truncation and filtering. Note that in panel 6d the patterns are almost the same for the case of filtering + truncation and the reversed order case, truncation + filtering, while in panel 6e the patterns are changed to a large extent. The noises near poles in Fig. 6(c) and the larger difference found in Fig. 6(e) are direct consequence of the violation of the pole condition by truncating a part of the expansion coefficients. Note that in Fig. 6(e) the filtering alleviates the discontinuity at poles to a considerably lower level.

3.3. Test on the filter equation with $v < 0$ (or reverse diffusion)

The filter in (2.1) gives a selective damping with the smaller scales are more damped than the larger. In this section, it will be focused on the filter equation with $v < 0$. (This may be called as a reverse diffusion, or a sharpening process instead of smoothing.) If the variables are expanded with the spherical harmonics, the spherical-harmonics coefficient of the filtered variable $w_{l,m}$ is given as

$$w_{l,m} = \frac{g_{l,m}}{R_{l,q}}, \tag{3.6}$$

$$R_{l,q} = 1 + v[l(l+1)]^q, \tag{3.7}$$

where $g_{l,m}$ is the spherical-harmonics coefficient of the forcing function $g(\lambda, \phi)$ and $l(= 0, 1, 2, \ldots)$ is the total wavenumber-like index. In principle, the filtered function can be calculated for an arbitrary filter viscosity v unless $R_{l,q}$ vanishes. The same must be true for the DFS expansion case. For the DFS method, however, the calculation of the same formula as in (3.7) does not appear explicitly, because the filtering is performed in terms of matrix inversion. Instead, the singularity will be reflected as either the vanishing diagonal components or off-diagonal dominance.

The DFS of (2.8) is applied to the filter equation with $v = -100/[N(N+1)]^q$ for $N = 64$. With this viscosity, the response function $R_{l,q}$ does not vanish for any l and q. The results are presented in Table 3, where the logarithm of the error ($\log_{10} E$) is shown for some selected zonal wavenumbers. The errors are almost the same as in Figs. 4 and 5. To see how the filter responses if the filter coefficient is taken such that the denominator vanishes, the same inversion as in Table 3 is carried out with $v = -1/[(N/2)(N/2+1)]^q$. It is found that the inversion is carried out without numerical overflow, but the errors become as large as the order of unity.

3.4. Inversion with a finite difference approximation in meridional direction

Since the high-order filter equation is solved in terms of successive inversion of the Helmholtz equation, the finite difference method (FDM) can also be applied to this problem. Although the main concern of this paper is the DFS spectral method, the solution of (2.1) is obtained with a finite difference approximation to demonstrate that the operator splitting method shown in Section 2 is quite useful. When a standard FDM is

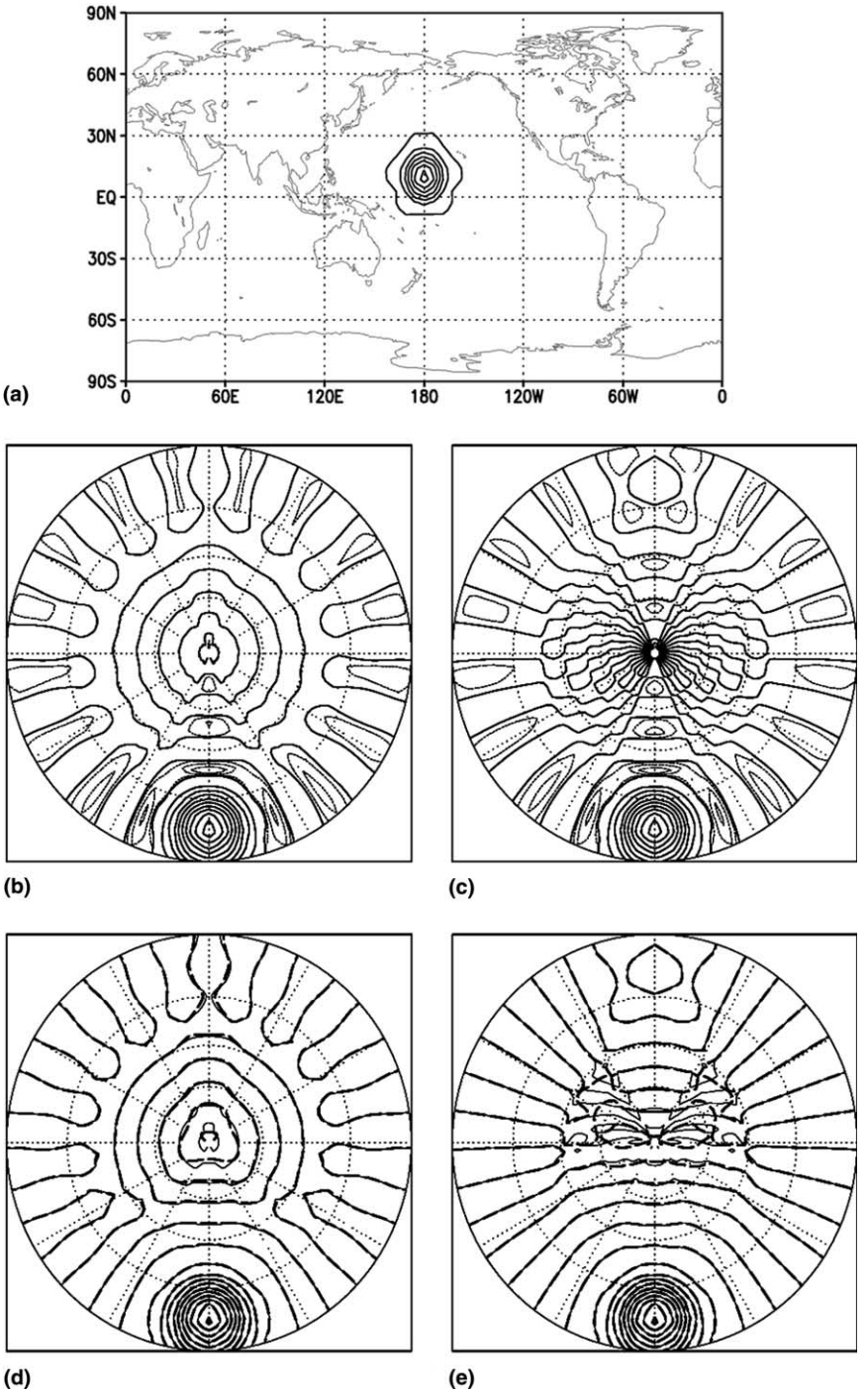

Fig. 6. (a) A cosine-bell shape function centered at (180E, 10N) with contour interval (CI) of 0.15 (distortion of the field is due to the map projection). (b) Truncated field using DFS in (2.8), where CI = 0.1 for positive values but broken lines are drawn at −0.0035, −0.0105 and −0.021. (c) Same as (b) except DFS of (2.11). (d) Thick broken lines (thin solid lines) with CI = 0.1 represent the result of *truncation + filtering* (*filtering + truncation*) with the use of (2.8). (e) The same as (d) but using (2.11).

Table 3
Logarithmic error ($\log_{10} E$) associated with the filter equation with a negative coefficient for the resolution of $N = 64$, where q represents the order of the filter equation

m	$q = 1$	$q = 2$	$q = 2$	$q = 4$
0	−14.0	−14.1	−14.3	−14.4
1	−14.5	−14.7	−15.0	−15.1
2	−14.5	−14.6	−15.0	−15.2
10	−13.6	−14.1	−14.8	−15.1
20	−12.8	−13.4	−14.5	−15.0

applied, the Helmholtz equation yields a huge block-diagonal matrix. To simplify the problem, the FDM is used only in the meridional direction. Finite difference approximation in meridional direction for the zonal Fourier transform of (2.4) yields [13,24]

$$(w_1)_{m,j} - \frac{\gamma_1}{\Delta^2 S_{j-0.5}}\left[S_j (w_1)_{m,j+1} + d_{m,j}(w_1)_{m,j} + S_{j-1}(w_1)_{m,j-1}\right] = g_{m,j} \quad (j = 1, 2, \ldots, N), \tag{3.8}$$

where

$$\Delta = \pi/N, \tag{3.9a}$$

$$S_j = \sin j\Delta, \tag{3.9b}$$

$$d_{m,j} = -(S_j + S_{j-1} + \Delta^2 S_{j-0.5}^{-1} m^2). \tag{3.9c}$$

As in DFS method, the global-mean correction should be done so that the global-means of the filtered variable and the forcing function are the same. In the FDM, the global-mean is obtained by a weighted sum of zonal-mean components

$$\left[w_{0,j} + \sum_{j=1}^{N} (g_{0,j} - w_{0,j}) W_j\right] \Rightarrow w_{0,j}, \tag{3.10a}$$

$$W_j = [\cos(j-1)\Delta - \cos j\Delta]/2. \tag{3.10b}$$

Errors are evaluated using the forcing function given in (3.1)–(3.3) for the fourth-order filter with the filter coefficient of $v = 100/[N/(N+1)]^q$. For fixed resolution the error ($\log_{10} E$) increases almost linearly with the zonal wavenumber, reaching near −1 at the highest zonal wavenumber. The error is smallest at zonal wavenumber of 0 or 1, which exhibits −11, −9, −7 and −5 for $N = 128$, 64, 32 and 16, respectively. The overall error would be larger than these if the zonal differentiation is also carried out with FDM. This method may be applicable to the FDM model on the sphere that incorporates the diffusion with a high-order Laplacian-operator, e.g. [20].

4. A simple and efficient HSF with pentadiagonal matrices

4.1. Biharmonic operator and pentadiagonal matrices

The major advantage of the new method over the method in [8] is the clarity and simplicity in the aspect of the numerical implementation for a practical use. The new method requires only the tridiagonal matrices

that are used for the inversion of Poisson's equation, therefore a rather complicated procedure to construct the pentadiagonal matrices as in [8] can be avoided. However, the computing time increases by a factor of about two, compared to the previous method.

In this section a high-order harmonic spectral filter, which is as simple as the new method and as efficient as the filter in [8], is presented which inverts pentadiagonal matrices. The key aspect of the filter is to construct the pentadiagonal matrices by manipulating the simple tridiagonal matrices in (2.12) of which elements are illustrated in Fig. 3. For this purpose a second-order differential operator is defined

$$L\{X\} \equiv \sin\phi \frac{\partial}{\partial\phi} \sin\phi \frac{\partial}{\partial\phi} X. \tag{4.1}$$

With this operator, the biharmonic operator can be written as

$$\nabla^4 X \equiv \frac{1}{\sin^2\phi}\left(L - m^2\right)\left\{\frac{1}{\sin^2\phi}\left[L\{X_m\} - m^2 X_m\right]\right\} \tag{4.2a}$$

$$\begin{aligned} &= \frac{-m^2}{\sin^4\phi}\left[L\{X_m\} - m^2 X_m\right] \\ &\quad + \frac{1}{\sin^2\phi} L\left\{\frac{1}{\sin^2\phi}\right\}\left[L\{X_m\} - m^2 X_m\right] + \frac{1}{\sin^4\phi} L\{L\{X_m\} - m^2 X_m\} \\ &\quad - \frac{2}{\sin^2\phi} L_1\{L\{X_m\} - m^2 X_m\}, \end{aligned} \tag{4.2b}$$

$$L_1 \equiv \frac{\sin 2\phi}{\sin^2\phi} \frac{\partial}{\partial\phi}, \tag{4.3}$$

where X_m is zonal Fourier transform of X and the operation of (4.1) to a quadratic term is used

$$L\left\{\frac{1}{\sin^2\phi} X\right\} = L\left\{\frac{1}{\sin^2\phi}\right\} X + \frac{1}{\sin^2\phi} L\{X\} - 2L_1\{X\}, \tag{4.4a}$$

$$L\left\{\frac{1}{\sin^2\phi}\right\} \equiv \left(-2 + \frac{4}{\sin^2\phi}\right). \tag{4.4b}$$

As shown in Eqs. (3.1)–(3.4) of [8], the filter operator (2.1) can be factorized into biharmonic and harmonic equations. Using the operations in (4.2b), the biharmonic equation is replaced by the pentadiagonal matrices equation, e.g.,

$$\sin^4\phi\left[1 + \gamma_1\nabla^2 + \gamma\nabla^4\right] w(\lambda,\phi) = \sin^4\phi\, g(\lambda,\phi), \tag{4.5a}$$

$$\Rightarrow \left[Z\mathbf{w} = A^2\mathbf{g}\right]. \tag{4.5b}$$

The matrix Z with the size of $N/2 \times N/2$ is given as

$$Z = A^2 + \gamma_1 AD + \gamma D_1 D \quad (D_1 \equiv D - 2A + 4I - 4B), \tag{4.6}$$

where I is unit diagonal and A and D are tridiagonal matrices shown in (2.12), and B is tridiagonal matrices of which elements are given in Fig. 7. Z is pentadiagonal matrix which can be calculated with ease. It is obvious that for the evaluation of Z one must prepare the matrices A, B and D with the size of $(N/2+1) \times (N/2+1)$. The simplicity of (4.6) is achieved by separating $(\sin\phi)^{-2}$ from the operand in

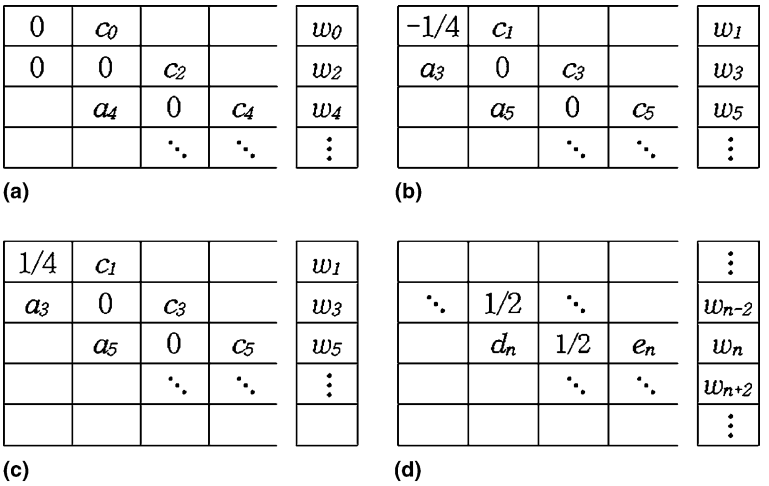

Fig. 7. (a)–(b) Matrix components of B for cosine series. (c) Sine series. (d) Modified sine series. The elements are given by $a_n = (n-2)/4$, $c_n = -(n+2)/4$, $d_n = (n-1)/4$ and $e_n = -(n+1)/4$.

(4.2a), which would result in a full matrix A^{-1} when a variable such as $(\sin\phi)^{-2}X$ is expanded with DFS. The pentadiagonal matrices Z in (4.6) should be identical to those obtained through a fourth-order differentiation as presented in [8]. This was confirmed by a direct comparison of the elements. However, the symmetric component for zonal-mean part is handled by the use of Legendre polynomials in [8]. In this case, the performance of the filter in (4.5b) was tested for the same problem in (3.1)–(3.3) instead of comparing the elements each other. The result showed the same order of accuracy as that given by the Legendre polynomials.

4.2. Efficiency of the HSF with pentadiagonal matrices

As to the efficiency of the filter with pentadiagonal matrices, it would be helpful to check the relative computing time to that needed for a spectral transform because the advantage of DFS model is characterized by the applicability of the fast algorithm to the spectral transform. For this purpose, a high performance computer NEC SX-5 was used, which consists of parallel vector processors with the vector register length of 512. The theoretical peak performance of a processor is 10 GFLOPS. The computations were performed on a single processor. Table 4 compares the real execution time for a spectral transform and a third-order (∇^6) spectral filtering. The truncation is given as in Section 2. That is, all wave components in (2.9) are retained. Note that the computing time for the spectral transform is considerably larger than that for the spectral filtering, typically by four or five times. The difference in computing time increases with the resolution. For the

Table 4
Real execution time for a spectral transform and a third-order spectral filtering, where $N(K)$ is the maximum wavenumber (the number of zonal grid points)

(N,K)	Spectral transform	Spectral filtering (∇^6)
$(256, 512)$	4.07	1.00
$(512, 1024)$	17.85	4.11
$(1024, 2048)$	81.50	17.40
$(2048, 4096)$	366.77	75.61

The computing time is normalized by that of the spectral filtering for $(N,K) = (256, 512)$.

time-dependent nonlinear problems, the number of spectral transforms is larger than that of the spectral filtering [6–8,10,19]. For example, the time stepping of the vorticity equation with DFS spectral method requires five spectral transforms and one spectral filtering per one timestep. In case of the shallow water equations nine spectral transforms and three times of spectral filtering are necessary per one timestep. The relative computing cost of the spectral filter varies depending on the order of the filter as well as the truncation. For example, if the truncation is given by the 2/3 rule as is usually done in the nonlinear model, the relative efficiency of the filter to the spectral transform is enhanced by a factor of 1.5 from those in Table 4. In any case, the additional computing cost due to the spectral filtering (*or* smoothing), even with the complex-valued matrices, is not significant for the DFS spectral transform method.

5. Summary and conclusions

In this paper the high-order harmonic spectral filter using double Fourier series on the sphere (HSF-DFS) was presented. The main concern of the paper is the simplicity of the filter in the aspect of numerical implementation for the practical use. The simplicity of the filter is achieved by either introducing a complex-valued tridiagonal matrix or constructing a pentadiagonal matrix with simple manipulation of tridiagonal matrices. For both cases, the direct fourth-order differentiation of the expansion functions shown in [8] is not necessary. The filters are tested for two commonly used uniform-grid system, the R-grid and S-grid (Fig. 1). Also presented is a detailed comparison of two double Fourier series focused on the pole conditions schematically illustrated in Fig. 2. Main results of the paper are summarized as following.

1. HSF-DFS consisting of the complex-valued tridiagonal matrices is easy and simple to construct, which consists of only the tridiagonal matrices required for the Poisson's equation solver. In comparison with the filter in [8], it provides the same order of accuracy whereas the computing time is doubled.
2. The pentadiagonal matrices for the filter in [8] can be constructed through simple manipulation of the tridiagonal matrices in Figs. 3 and 7. This was made possible by separating the fourth-order differential operator into three terms as shown in (4.2b). The computing cost for the spectral filtering (smoothing), even with the complex-valued matrices, is not significant compared to the spectral transform that constitute a central part of the DFS spectral transform method.
3. HSF-DFS can be applied to the uniform-grid systems regardless of inclusion of the poles as data points with the same order of accuracy. For both grid systems, DFS constitutes the alias-free complete set for the spectral expansion.
4. A DFS which incorporates the basis functions violating the pole conditions was found to be of no problematic when it is used without wave truncation. However, in case where it is used with some wave components eliminated, the small-scale noises are produced near poles due to the discontinuity of basis functions.
5. A reverse filter (diffusion), realized by using a negative diffusion coefficient, performs as accurate as the usual filter only if the coefficient is determined in such a way that the response function in (3.7) does not vanish.

With the operator splitting as in Section 2.1 the high-order HSF can be approximated with FDM or others (e.g., finite element method) which are considered to be not suitable for high-order differentials, because it is solved by inversion of successive Helmholtz equations without taking directly an approximation of the high-order differentials.

Acknowledgements

This work was supported by Grant No. R05-2002-000214-0 from the Basic Research Program of the Korea Science and Engineering Foundation. The authors would like to acknowledge the support from

the Korea Institute of Science and Technology Information (KISTI) under 'the 3rd Strategic Supercomputing Applications Support Program'. A part of the computations in this study was performed on the computing system SX-5 of Supercomputing Center at KISTI.

Appendix A. Spectral transform of modified sine series and pole conditions

To avoid the singularity at the time of spectral transform in case of R-grid, the modified sine series for even $m(\neq 0)$ are replaced by the cosine series with the maximum wavenumber increased by one-level

$$\sum_{n=1}^{N_c} g_{n,m} \sin\phi \sin n\phi = \sum_{n=0}^{N_c+1} C_{n,m} \cos n\phi, \tag{A.1}$$

where the completeness requirement of the cosine-series expansion as in (2.9), $N_c + 1 = N_o(\equiv N)$ is satisfied, implying that the modified sine expansion is free of the aliasing (being equivalence between two series). One important issue for this replacement is that the cosine series should satisfy the pole condition as the modified sine series does. Since the differentiation (see Fig. 2) at poles vanishes, the remaining one, the condition of vanishing value at poles (i.e., $g_m(\phi) = 0$) is of concern.

Both coefficients $g_{n,m}$ and $C_{n,m}$ are interrelated with the recursion relation, which yields for $2 \leqslant n \leqslant N-2$ (the subscript m is dropped)

$$C_n = (g_{n+1} - g_{n-1})/2 \tag{A.2a}$$

or

$$g_{n+1} = g_{n-1} + 2C_n, \tag{A.2b}$$

and for particular indices

$$C_0 = +g_1/2, \tag{A.3a}$$

$$C_1 = +g_2/2, \tag{A.3b}$$

$$C_{N-1} = -g_{N-2}/2, \tag{A.3c}$$

$$C_N = -g_{N-1}/2. \tag{A.3d}$$

In the spectral transform procedure, the cosine transform is performed to get $C_{n,m}$ as a first step, and the coefficients $g_{n,m}$ are obtained using the recursion relations above either by descending or ascending order. The results calculated with the ascending and descending order are the same, due to the constraint on the spectral coefficients arising from the pole condition. The sum of the cosine expansion coefficients $C_{n,m}$ must vanish for each zonal wavenumber in order that the pole condition as in Fig. 2 is satisfied. The pole condition can be written in terms of the expansion coefficients as

$$\left[\sum_{n=0}^{N_c+1} C_{n,m}\right]_{(n=\text{even})} = \left[\sum_{n=1}^{N_c} C_{n,m}\right]_{(n=\text{odd})} = 0. \tag{A.4}$$

This is trivially satisfied because $g_m(0) = g_m(\pi) = 0$ for even $m(\neq 0)$ in case of the R-grid, because the poles are data point and the interpolativeness between the wave-components and the grid-point data are

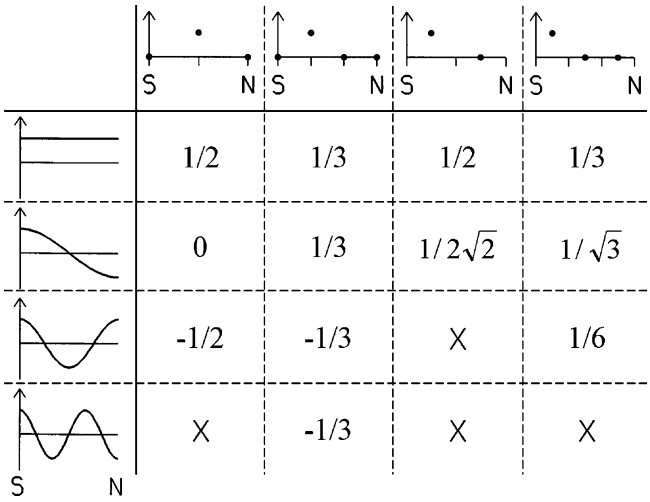

Fig. 8. Fourier coefficients of the cosine expansion for the even zonal wavenumber. Extremely low resolution case in meridian is illustrated for clarity. The curves represent the cosine waves, and the uppermost row denotes the grid-point data for the R-grid (the first two maps) and S-grid (the last two). The grid-point values are either unity or zero. The mark '×' implies that the wave component is not available due to the truncation limit. Note that the sum of wave components for R-grid (S-grid) vanishes (does not vanish). In each case, the normalization factor is given the same for the lowest and the highest wavenumber component.

guaranteed. The last two components g_{N-2} and g_{N-1} can be determined either by (A.2b) or Eqs. (A.3c) and (A.3d), because the condition in (A.4) gives

$$C_{N-1} = -\left[\sum_{n=1}^{N-3} C_n\right]_{(n=\text{odd})}, \tag{A.5a}$$

$$C_N = -\left[\sum_{n=0}^{N-2} C_n\right]_{(n=\text{even})}. \tag{A.5b}$$

Note that if even one spectral component with non-zero value is removed from $C_{n,m}$, the pole condition (A.4) is violated. With some components of $C_{n,m}$ being deleted, the recursion relation (A.2a), (A.2b) becomes incomplete so that $g_{n,m}$ cannot be determined uniquely from $C_{n,m}$. The pole condition (A.4) is not trivially satisfied in case of S-grid even when all the spectral components are incorporated because the poles are not the data point. This situation is illustrated in Fig. 8 with simple grid systems.

References

[1] G.J. Boer, L. Steinberg, Fourier series on spheres, Atmosphere 13 (1975) 180–191.
[2] Y. Bouteloup, Improvement of the spectral representation of the earth topography with a variational method, Monthly Weather Rev. 123 (1995) 1560–1573.
[3] J.P. Boyd, Chebyshev and Fourier Spectral Methods, second ed., Dover, New York, 2001, 688 pp.
[4] T. Bulow, Reverse diffusion for smooth buildup of progressively transmitted geometry, Preprint of Eurographics 2002, Saarbruecken, Germany, 2002.
[5] C. Catuno, M.Y. Hussaini, A. Quarteroni, T.A. Zang, Spectral Methods in Fluid Dynamics, Springer-Verlag, New York, 1988, 567 pp.

[6] H.-B. Cheong, Double Fourier series on a sphere: applications to elliptic and vorticity equations, J. Comput. Phys. 157 (2000) 327–349.
[7] H.-B. Cheong, Application of double Fourier series to shallow water equations on a sphere, J. Comput. Phys. 165 (2000) 261–287.
[8] H.-B. Cheong, I.-H. Kwon, T.-Y. Goo, M.-J. Lee, High-order harmonic spectral filter with the double Fourier series on a sphere, J. Comput. Phys. 177 (2002) 313–335.
[9] H.-B. Cheong, Y.-C. Song, I.-H. Kwon, Inversion of global linear balance equation with the spectral method using the spherical harmonics and double Fourier series, Monthly Weather Rev. (2003), submitted.
[10] A. Gleb, J. Gleeson, Spectral viscosity for shallow water equations in spherical geometry, Monthly Weather Rev. 129 (2001) 2346–2360.
[11] E. Kalnay et al., The NCEP/NCAR 40-year reanalysis project, Bull. Amer. Met. Soc. 77 (1996) 437–731.
[12] S.-G. Kim, W.-T. Kim, T. Suzuki, Phase-field model for binary alloys, Phys. Rev. E 60 (1999) 7186–7197.
[13] M.-C. Lai, W.-C. Wang, Fast direct solvers for Poisson equation on 2D polar and spherical geometries, Numer. Methods Partial Differential Equtions 18 (2002) 56–68.
[14] L. Laursen, E. Eliasen, On the effects of the damping mechanisms in an atmospheric general circulation model, Tellus A 41 (1989) 385–400.
[15] A.T. Layton, W.F. Spotz, A semi-Lagrangian double Fourier method for the shallow water equations on the sphere, J. Comput. Phys. 189 (2003) 180–196.
[16] Jia Li, Three dimensional shape modeling: Segmentation, reconstruction and registration, A Ph.D. Dissertation, Department of Electrical Engineering and Computer Science, University of Michigan, 2002, 153 pp.
[17] S.A. Orszag, Fourier series on spheres, Monthly Weather Rev. 102 (1974) 56–75.
[18] W.H. Press, S.A. Teukolsky, W.T. Vetterling, B.P. Flannery, Numerical Recipes in FORTRAN, Cambridge University Press, Cambridge, MA, 1992, 963 pp.
[19] L. Rivier, R. Loft, L.M. Polvani, An efficient spectral dynamical core for distributed memory computer, Monthly Weather Rev. 130 (2001) 1384–1396.
[20] C. Ronchi, R. Iacono, P.S. Paolucci, The "cubed sphere": a new method for the solution of partial differential equations in spherical geometry, J. Comput. Phys. 124 (1996) 93–114.
[21] P.D. Sardeshmukh, B.J. Hoskins, Spatial smoothing on the sphere, Monthly Weather Rev. 112 (1984) 2524–2529.
[22] A.J. Simmons, D.M. Burridge, M. Jarraud, C. Girard, W. Wergen, The ECMWF medium-range prediction models: development of the numerical formulations and the impact of the increased resolution, Meteorol. Atmos. Phys. 40 (1989) 28–60.
[23] W.F. Spotz, M.A. Taylor, P.N. Swarztrauber, Fast shallow water equation solvers in latitude–longitude coordinates, J. Comput. Phys. 145 (1998) 432–444.
[24] P.N. Swarztrauber, The direct solution of the discrete Poisson equation on the surface of a sphere, J. Comput. Phys. 15 (1974) 46–54.
[25] S.Y.K. Yee, Solution of Poisson's equation on a sphere by truncated double Fourier series, Monthly Weather Rev. 109 (1981) 501–505.